

## A Solid State $^{13}\text{C}$ NMR, Crystallographic, and Quantum Chemical Investigation of Phenylalanine and Tyrosine Residues in Dipeptides and Proteins

Dushyant Mukkamala,<sup>†</sup> Yong Zhang,<sup>‡</sup> and Eric Oldfield<sup>\*,†,‡</sup>

Contribution from the Center for Biophysics and Computational Biology, 607 South Mathews Avenue, University of Illinois at Urbana-Champaign, Urbana, Illinois 61801, and Department of Chemistry, University of Illinois at Urbana-Champaign, 600 South Mathews Avenue, Urbana, Illinois 61801

Received February 20, 2007; E-mail: eo@chad.scs.uiuc.edu

**Abstract:** We report the results of a solid-state NMR and quantum chemical investigation of the  $^{13}\text{C}^\gamma$  NMR chemical shifts in phenylalanine and tyrosine in dipeptides and proteins. Accurate computation of the experimental shifts is shown to require a good description of local electrostatic field effects, and we find the best results ( $R^2 = 0.94$ , rmsd = 1.6 ppm, range = 17.1 ppm,  $N = 14$ ) by using a self-consistent reaction field continuum model. There are no obvious correlations with  $\phi$ ,  $\psi$ ,  $\chi_1$ , or  $\chi_2$  torsion angles, unlike the results seen with other amino acids. There is, however, a linear relation between computed  $\text{C}^\gamma$  atomic charges and shifts for the 14 peptide as well as 18 protein residues investigated. This result is similar to the correlation reported in the 1960s between  $\pi$ -electron density and  $^{13}\text{C}$  shifts for classical  $4n + 2$  ( $n = 0, 1, 2$ )  $\pi$ -electron aromatic species, such as cyclopentadienide and the tropylium cation, and in fact, we found that the shielding/atomic charge correlation seen in the peptides and proteins is virtually identical to that seen with a broad range of aromatic carbocations/carbanions. These results suggest the dominance of an electrostatic field polarization model in which increasing  $\pi$  electron density results in an increase in  $\text{C}^\gamma$  atomic charge and increased shielding (of  $\sigma_{11}$  and  $\sigma_{22}$ , perpendicular to the  $\pi$  orbital) in Phe and Tyr, as well as in the other aromatic species. These results are of general interest since they demonstrate the importance of electrostatic field effects on Phe and Tyr  $\text{C}^\gamma$  chemical shifts in peptides and proteins and imply that inclusion of these effects will be necessary in order to interpret the shifts of other aromatic species, such as drug molecules, bound to proteins.

### Introduction

Folding a protein into its native conformation causes a large range of chemical shift nonequivalence, of obvious importance from the perspective of NMR structure determination. For  $^1\text{H}$ , chemical shifts due to folding are typically about 2 ppm; for  $^{13}\text{C}$ , chemical shift ranges due to folding are typically  $\sim 10$  ppm; for  $^{19}\text{F}$  (in labeled proteins),  $\sim 20$  ppm, and for  $^{15}\text{N}$ , up to about 35 ppm. For  $^1\text{H}$ , quite good correlations have been found between experiment and prediction using, e.g., ring-current shifts and empirical descriptions of electrostatics, but for the heavier nuclei,  $^{13}\text{C}$ ,  $^{15}\text{N}$ , and  $^{19}\text{F}$ , quantum chemical methods have to be used.<sup>1</sup> In previous work, we found that backbone ( $^{13}\text{C}^\alpha$ ) shifts were dominated by electronic effects due to  $\phi$ ,  $\psi$  differences, and in sidechains,  $\chi_1/\chi_2$  or other (gamma-gauche) effects contribute to shielding. Similar conformational contributions were found to dominate  $^{15}\text{N}$  shifts,<sup>1–3</sup> but for  $^{19}\text{F}$  in aromatic amino acids,<sup>1,4,5</sup> purely electrostatic field effects dominated shielding, since backbone or side chain torsional effects for say

a [ $5\text{-}^{19}\text{F}$ ] Trp labeled protein would clearly be too long-range to affect  $^{19}\text{F}$  shifts directly. The results of a number of investigations have shown that most chemical shifts in proteins (including metal shifts and paramagnetic or hyperfine shifts) can now be computed with good accuracy,<sup>6,7</sup> but a remaining problem has been that of  $\text{C}^\gamma$  of the aromatic amino acids, phenylalanine, and tyrosine. The shift ranges for  $\text{C}^\gamma$  in Phe and Tyr were found in early studies<sup>8</sup> to be quite small ( $\sim 3\text{--}4$  ppm), but the shifts of Trp residues<sup>8,9</sup> were much larger ( $\sim 6\text{--}7$  ppm), and this enhanced shift range facilitates the overall precision (versus experiment) of quantum chemical shielding predictions, which are typically  $\sim 1\text{--}2$  ppm for Trp  $\text{C}^\gamma$ .<sup>2</sup> Here, we report the first  $^{13}\text{C}$  NMR chemical shift predictions for  $\text{C}^\gamma$  in Phe and Tyr residues, both in dipeptides and in proteins. Unlike  $\text{C}^\alpha$  (and  $\text{C}^\beta$ ), there are no obvious correlations with either the backbone torsion angles or  $\chi_1/\chi_2$ . Rather, our results suggest that electrostatic field effects make an important contribution to shielding

<sup>†</sup> Center for Biophysics and Computational Biology.

<sup>‡</sup> Department of Chemistry.

- (1) de Dios, A. C.; Pearson, J. G.; Oldfield, E. *Science* **1993**, *260*, 1491.
- (2) Sun, H.; Oldfield, E. *J. Am. Chem. Soc.* **2004**, *126*, 4726.
- (3) Szabo, C. M.; Sanders, L. K.; Le, H. C.; Chien, E. Y.; Oldfield, E. *FEBS Lett.* **2000**, *482*, 25.

- (4) Pearson, J. G.; Montez, B.; Le, H.; Oldfield, E.; Chien, E. Y.; Sligar, S. G. *Biochemistry* **1997**, *36*, 3590.
- (5) Pearson, J. G.; Oldfield, E.; Lee, F. S.; Warshel, A. *J. Am. Chem. Soc.* **1993**, *115*, 6851.
- (6) Mao, J.; Zhang, Y.; Oldfield, E. *J. Am. Chem. Soc.* **2002**, *124*, 13911.
- (7) Zhang, Y.; Sun, H.; Oldfield, E. *J. Am. Chem. Soc.* **2005**, *127*, 3652.
- (8) Oldfield, E.; Norton, R. S.; Allerhand, A. *J. Biol. Chem.* **1975**, *250*, 6381.
- (9) Oldfield, E.; Allerhand, A. *J. Biol. Chem.* **1975**, *250*, 6403.

and that use of a “solvent” (self-consistent reaction field, SCRF) model enables the best accord with experiment. Remarkably, we also find that the computed shifts are highly correlated with  $C^\gamma$  atomic charges, reminiscent of the correlations reported many years ago<sup>10–14</sup> between  $^{13}\text{C}$  shifts and  $\pi$ -electron densities in a variety of other classical aromatic  $4n + 2$   $\pi$ -electron systems.

## Experimental Details

**NMR Spectroscopy:**  $^{13}\text{C}$  NMR spectra were obtained by using the cross-polarization “magic-angle” sample-spinning technique<sup>15,16</sup> with either full proton decoupling<sup>17</sup> or interrupted decoupling<sup>18</sup> (using a dipolar dephasing time of 140  $\mu\text{s}$  for phenylalanine and tyrosine residues), for selection of the nonprotonated aromatic carbons ( $C^\gamma$  and  $C^\delta$ ). The  $^1\text{H}$  and  $^{13}\text{C}$  90° pulse widths used were 2.6  $\mu\text{s}$ , and the spectra in all cases were collected using a recycle time of 5 s. The chemical shifts were referenced to external glycine, setting the Gly  $C^\alpha$  carbon to 43.6 ppm downfield from tetramethylsilane (TMS). All the experiments were performed on a Varian (Palo Alto, CA) Infinityplus 600 MHz ( $^1\text{H}$ ) NMR spectrometer at a 10 kHz spinning speed using a 3.2 mm Varian/Chemagnetics HXY probe. Fully  $^1\text{H}$  decoupled experiments were carried out at two different spinning speeds (8 kHz and 10 kHz), in order to determine the isotropic chemical shifts. The compounds for the NMR experiments were obtained from Bachem (King of Prussia, PA).

**X-ray Crystallography.** The structures of the 11 compounds (1–11) investigated are shown in Supporting Information Figure S1. To verify their actual structures, we obtained powder diffraction data for each system and compared the results with calculated powder spectra for crystal structures obtained from the Cambridge Crystallographic Data Center (CCDC). The powder spectra for each sample were calculated by using DIFFRACplus TOPAS.<sup>19</sup> For six dipeptides (1, 2, 4, 7–9), we found a very good match between the calculated and experimental powder diffraction data, so these structures were used directly in the calculations. For three compounds (3, 5, 10), we obtained a good match between the computed and experimental diffraction results after refining the unit-cell parameters using the Pawley fitting method,<sup>20</sup> as incorporated in DIFFRACplus TOPAS.<sup>19</sup> The experimental and calculated powder patterns for two compounds (6, 11) did not match those reported, so we recrystallized them and determined their structures by X-ray crystallography. Compound 6 was crystallized from water, while 11 was crystallized from 5% DMSO–water, and the structures so obtained are shown in Figure 1a,b. Full crystallographic details are given in Table S1 in the Supporting Information.

**Computational Aspects:** We performed eight sets of calculations in order to compute the  $^{13}\text{C}$  NMR shieldings for the phenylalanine and tyrosine dipeptides (1–11) shown in Figure S1. In six cases, we used the Hartree–Fock method as incorporated in Gaussian 98<sup>21</sup> and Gaussian 03,<sup>22</sup> using the locally dense basis set scheme (6-311++G (2d,2p)/6-31G\*) with the denser basis set on the atoms of interest (and their nearest neighbors), combined with the gauge-including atomic orbitals (GIAO) method.<sup>23</sup> The first set of calculations utilized the *N*-formyl-phenylalanine-amide model approach<sup>1</sup> (Figure 1c), the same

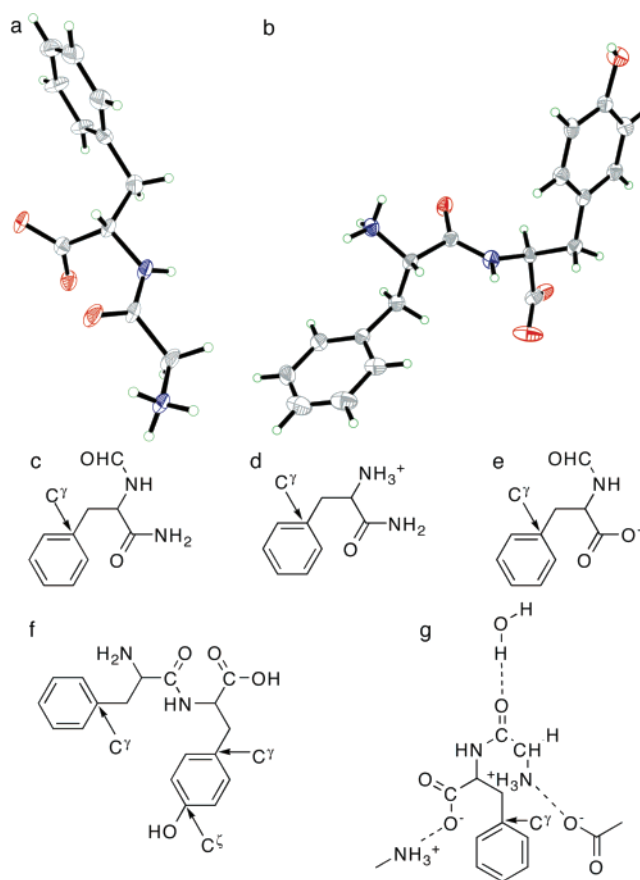


**Figure 1.** Structures and models: (a) Crystal structure of compound 6; (b) crystal structure of compound 11; (c) *N*-formyl-phenylalanine-amide model; (d) *N*-terminus charged model; (e) *C*-terminus charged model; (f) monomer from crystal structure of Phe-Tyr (11); and (g) monomer from crystal structure of Gly-Phe (6) with surrounding hydrogen-bond partners.

approach as that used in studying tryptophan chemical shifts,<sup>2</sup> with the torsion angles ( $\phi$ ,  $\psi$ ,  $\chi_1$ , and  $\chi_2$ , as appropriate) set to the values seen in the X-ray structures. After this, we performed calculations on charged models of the *N*-formyl-phenylalanine-amide structures, converting the terminal *N*-formyl group to  $\text{NH}_3^+$  or the amide to  $\text{CO}_2^-$ , for *N*-terminal and *C*-terminal models, respectively (Figure 1d and e). The next set of calculations used the monomers found in the X-ray crystal structures, as shown for example in Figure 1f. In the fourth set of calculations, we used hydrogen-bond partner cluster models in which the effects of neighboring residues were included by incorporating acetate or methylammonium ions, or formamide or methanol molecules, to represent the lattice partners, e.g., Figure 1g. And, in the case of tyrosine, since some structures had what appeared to be bad ( $\sim 0.6$  Å) OH bond lengths, we performed geometry optimization of the  $C^\delta$  hydroxyl group (using the HF method and a locally dense basis set scheme, 6-311++G (2d,2p)/6-31G\*).

In the case of phenylalanine, we also used charge field perturbation<sup>24</sup> to simulate nearest neighbor interactions, in which additional molecules are represented by just point charges, rather than by real atoms.<sup>25,26</sup> The charge lattices for the crystal structures were generated by using the Shelxtl program,<sup>27</sup> and we used the electrostatic potential (ESP) derived MK (Merz–Kollman)<sup>28</sup> charges provided in Gaussian 03. For

(10) LaLancette, E. A.; Benson, R. E. *J. Am. Chem. Soc.* **1965**, *87*, 1941.

(11) Olah, G. A.; Bollinger, J. M.; White, A. M. *J. Am. Chem. Soc.* **1969**, *91*, 3667.

(12) Olah, G. A.; Mateescu, G. D. *J. Am. Chem. Soc.* **1970**, *92*, 1430.

(13) Spiess, H.; Schneider, W. G. *Tetrahedron Lett.* **1961**, *2*, 468.

(14) Weigert, F. J.; Roberts, J. D. *J. Am. Chem. Soc.* **1967**, *89*, 2967.

(15) Pines, A.; Gibby, M. G.; Waugh, J. S. *J. Chem. Phys.* **1973**, *59*, 569.

(16) Schaefer, J.; Stejskal, E. O. *J. Am. Chem. Soc.* **1976**, *98*, 1031.

(17) Bennett, A. E.; Rienstra, C. M.; Auger, M.; Lakshmi, K. V.; Griffin, R. G. *J. Chem. Phys.* **1995**, *103*, 6951.

(18) Opella, S. J.; Frey, M. H. *J. Am. Chem. Soc.* **1979**, *101*, 5854.

(19) DIFFRACplus TOPAS, 3.0 ed.; Bruker AXS, 2005.

(20) Pawley, G. S. *J. Appl. Crystallogr.* **1981**, *14*, 357.

(21) Frisch, M. J., et al. *Gaussian 98*; Gaussian, Inc.: Pittsburgh, PA, 1998.

(22) Frisch, M. J., et al. *Gaussian 03*; Gaussian, Inc.: Pittsburgh, PA, 2003.

(23) Ditchfield, R. *Mol. Phys.* **1974**, *27*, 789.

(24) de Dios, A. C.; Oldfield, E. *Chem. Phys. Lett.* **1993**, *205*, 108.

(25) Arnold, W. D.; Sanders, L. K.; McMahon, M. T.; Volkov, A. V.; Wu, G.; Coppens, P.; Wilson, S. R.; Godbout, N.; Oldfield, E. *J. Am. Chem. Soc.* **2000**, *122*, 4708.

(26) de Dios, A. C.; Laws, D. D.; Oldfield, E. *J. Am. Chem. Soc.* **1994**, *116*, 7784.

(27) Shelxtl, version 6.12; Bruker AXS, 2000.

(28) Besler, B. H.; Merz, K. M.; Kollman, P. K. *J. Comput. Chem.* **1990**, *11*, 431.

both phenylalanine and tyrosine, we also employed a self-consistent reaction field theory (SCRF) “solvent” model<sup>29,30</sup> in order to see if this improved the quality of the shift/shielding predictions. We also carried out density functional theory (DFT) calculations using the hydrogen-bond “supermolecule” cluster models as well as the continuum models, using the B3LYP<sup>31–35</sup> functional and the same basis set scheme as that used in the Hartree–Fock calculations. And finally, we used the hydrogen-bond partner supermolecule cluster models along with the SCRF approach to evaluate the C<sup>γ</sup> chemical shifts of phenylalanine and tyrosine residues in four proteins (shifts from the BioMagRes Bank;<sup>36</sup> PDB Files: 1CZP, 2Fe-2S ferredoxin; 1EY0, staphylococcal nuclease; 1MO1, crh dimer and 3LZT, hen egg-white lysozyme).

## Results and Discussion

We first obtained the solid-state <sup>13</sup>C NMR spectra of each of the 13 phenylalanine- and 15 tyrosine-containing dipeptides shown in Figure S1, in order to assess the range in experimental chemical shifts that might be seen in model systems. Spectra were recorded either with full proton decoupling or by using interrupted decoupling, in order to select for the nonprotonated (C<sup>γ</sup>, C<sup>δ</sup>) aromatic carbon sites. In the case of tyrosine, the most shielded nonprotonated peaks were assigned to C<sup>γ</sup>. Two representative spectra, those of Gly-Phe (**6**) and Tyr-Glu (**7**), are shown in Figure 2a–d. The entire list of C<sup>γ</sup> chemical shifts (compounds **1–26**; two contain both Phe and Tyr) is shown in Table 1 (all the Tyr C<sup>δ</sup> shifts are shown in the Supporting Information, Table S2). The C<sup>γ</sup> shift results obtained demonstrate a clear separation of the experimental chemical shifts into two distinct regions, depending on whether the phenylalanine/tyrosine residue is located at the N-terminus or at the C-terminus of the dipeptide. As can be seen in Figure 2e and f, N-terminal residues are always more shielded than are C-terminal residues. This pattern was not immediately apparent in the tryptophan and histidine dipeptides investigated earlier,<sup>2,38</sup> but on closer examination of the shifts of histidine (within the same tautomeric forms), we now find the same trend for His C<sup>γ</sup>, Table S3 of the Supporting Information. The trends seen in Phe and Tyr are, however, clearly less apparent with His and Trp, due most likely to the presence of heteroatoms in the His and Trp rings which contribute either to tautomerism (His),  $\chi_1$ – $\chi_2$  conformational contributions to shielding, and, in some cases, strong hydrogen bonding to a ring nitrogen close to C<sup>γ</sup>. Such contributions to shielding are of course absent in Phe and Tyr, and the C<sub>N</sub>-terminal effects dominate the overall shielding pattern seen experimentally.

The experimental C<sup>γ</sup> shift range in the phenylalanine dipeptides is ~7.0 ppm, Figure 2e, considerably larger than the 3.7 ppm shift range (Figure 2g) observed in 10 proteins. In the tyrosine dipeptides, the C<sup>γ</sup> shift range in peptides is 9.4 ppm, Figure 2f, while that for 10 proteins is 7.2 ppm (Figure 2h). So, the shift range seen in the dipeptides is ~2–3 ppm larger

than that seen in proteins. Also, as can be seen in Figure 2g and h, the protein shifts form a continuous “band” at the center of the shift range observed in the dipeptides. These results strongly suggest that, in addition to conformational effects influencing shifts, it is likely that electrostatic field effects (due to the proximity of the charged terminal groups) may be important in the dipeptides and that the shift range is actually dominated by these effects. As alluded to above, these results are in sharp contrast to those seen in Trp- and His- containing peptides where we find larger shift ranges (Trp C<sup>γ</sup>, 11.4 ppm; His C<sup>γ</sup>, 12.7 ppm; His C<sup>δ2</sup>, 13.8 ppm).

In order to obtain a more quantitative analysis of the Phe, Tyr C<sup>γ</sup> shifts, we chose to study 11 phenylalanine- and tyrosine-containing dipeptides, whose chemical shifts were representative of the observed shift ranges, using quantum chemical methods. For Phe, we first used *N*-formyl-phenylalanine-amide model calculations using the HF method and a locally dense basis set (6-311++G(2d,2p)/6-31G\*), the same approach as that used previously for proteins and peptides. These models take into account the effects on shielding of backbone ( $\phi$  and  $\psi$ ) and side-chain ( $\chi_1$  and  $\chi_2$ ) conformations. The calculated shieldings did not correlate with experiment, an unusual observation given that this approach has been successful in essentially all of our other <sup>13</sup>C shielding predictions. For example, the experimental C<sup>γ</sup> chemical shift in **Phe-Pro (1)** was 6.2 ppm more shielded than that in **Gly-Phe (6)**, but, with this model, the calculated **Phe-Pro (1)** C<sup>γ</sup> chemical shielding was 3.1 ppm more deshielded than that calculated for C<sup>γ</sup> **Gly-Phe (6)**. This suggests that there are effects other than  $\phi$ ,  $\psi$ ,  $\chi_1$ , or  $\chi_2$  angle dependence which dominate shielding in these dipeptides. Since the experimental shifts indicate, qualitatively, a strong dependence on whether a residue is at the N- or C-terminus, we next performed calculations on charged species: NH<sub>3</sub><sup>+</sup>-phenylalanine-amide models for the N-terminal residues and the *N*-formyl-phenylalanine-CO<sub>2</sub><sup>−</sup> models for the C-terminal residues. The results of these calculations (Supporting Information, Table S4) now begin to reproduce the shift trends observed experimentally, as can be seen in Figure 3a, but clearly the shifts occur in two pronounced clusters (corresponding to the N and C terminal residues) and the slope of the correlation line (−5.32) is unacceptable. So we next proceeded to calculations using the entire peptide monomers in the crystal structures. The results (Supporting Information, Table S5) provide an improvement in slope (−3.58), although this value is still very poor, strongly suggesting the importance of incorporating intermolecular interactions, as observed previously in the case of histidine dipeptide shielding calculations.<sup>38</sup> Using hydrogen-bond partner “supermolecule” clusters, the results (Supporting Information, Table S6) show further improvement (slope = −2.44) over the crystal structure calculations without hydrogen-bond partners. We also tried another approach to simulate the intermolecular interactions, charge-field perturbation,<sup>24</sup> but since the preliminary results from these calculations were very similar to those obtained from the crystal structure calculations (without hydrogen-bond partners), we did not pursue them further. In addition to the Hartree–Fock calculations on the hydrogen-bond partner “supermolecule” clusters, we also performed a series of DFT calculations using the hybrid functional B3LYP<sup>31–35</sup> (Supporting Information, Table S7). There was a slight improvement in slope (−2.11), but the correlation was slightly worse than that with

(29) Cossi, M.; Barone, V.; Cammi, R.; Tomasi, J. *Chem. Phys. Lett.* **1996**, 255, 327.

(30) Miertus, S.; Scrocco, E.; Tomasi, J. *Chem. Phys.* **1981**, 55, 117.

(31) Adamo, C.; Barone, V. *J. Chem. Phys.* **1998**, 108, 664.

(32) Becke, A. D. *Phys. Rev. A* **1988**, 38, 3098.

(33) Becke, A. D. *J. Chem. Phys.* **1993**, 98, 5648.

(34) Lee, C.; Yang, W.; Parr, R. G. *Phys. Rev. B* **1988**, 37, 785.

(35) Perdew, J. P.; Burke, K.; Wang, Y. *Phys. Rev. B* **1996**, 54, 16533.

(36) Seavey, B. R.; Farr, E. A.; Westler, W. M.; Markley, J. L. *J. Biomol. NMR* **1991**, 1, 217.

(37) Berman, H. M.; Westbrook, J.; Feng, Z.; Gilliland, G.; Bhat, T. N.; Weissig, H.; Shindyalov, I. N.; Bourne, P. E. *Nucleic Acids Res.* **2000**, 28, 235.

(38) Cheng, F.; Sun, H.; Zhang, Y.; Mukkamala, D.; Oldfield, E. *J. Am. Chem. Soc.* **2005**, 127, 12544.

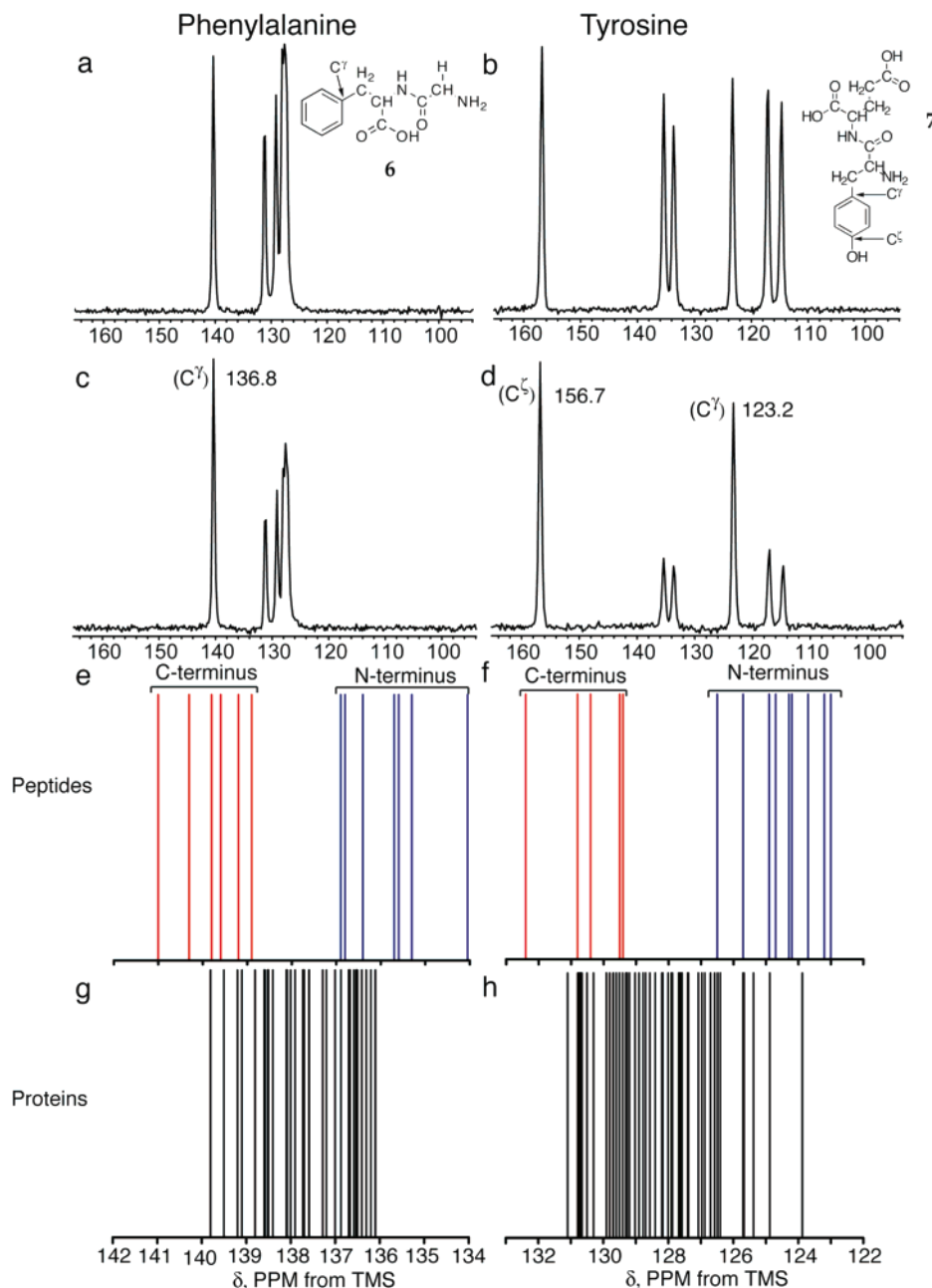


**Figure 2.** Carbon-13 NMR spectra and shifts in peptides and proteins: (a)  $^{13}\text{C}$  MAS NMR spectrum of Gly-Phe (**6**) with full proton decoupling; (b)  $^{13}\text{C}$  MAS NMR spectrum of Tyr-Glu (**11**) with full proton decoupling; (c)  $^{13}\text{C}$  MAS NMR spectrum of Gly-Phe (**6**) with interrupted decoupling; (d)  $^{13}\text{C}$  MAS NMR spectrum of Tyr-Glu (**11**) with interrupted decoupling; (e) Phe  $\text{C}^\gamma$  chemical shift distribution in dipeptides: blue, N-terminal residues; red, C-terminal residues; (f) Tyr  $\text{C}^\gamma$  chemical shift distribution in dipeptides: blue, N-terminal residues; red, C-terminal residues; (g) Phe  $\text{C}^\gamma$  chemical shift distribution in proteins. Data from the BMRB for: cytochrome c; microviridin; tendamistat; hen egg white lysozyme; micrococcal nuclease; staphylococcal nuclease; cutinase; protein disulfide isomerase; microcin J25; winged helix domain of c-Qin; crh dimer, and hath domain of hepatoma-derived growth factor.

the Hartree–Fock method ( $R = 0.79$  versus 0.81), offering no obvious improvement.

So, these chemical shift/shielding results appear to be the poorest correlations between theory and experiment we have observed so far, and there has to be a reason for this. Since  $\text{C}^\gamma$  is quite distal to the peptide backbone,  $\phi, \psi$  effects are expected to be small. There could be  $\chi_1/\chi_2$  effects, but note here that, unlike Trp and His, due to the absence of a heteroatom in the Phe or Tyr ring, a  $180^\circ$  flip of a Phe or Tyr ring has no effect on shielding, while a rotation about  $\text{C}^\beta\text{—}\text{C}^\gamma$  will have marked effects on shielding, in His and Trp. Moreover, any hydrogen-bond interaction with the heteroatoms in the His and Trp

imidazole/indole rings is expected to have a significant effect on shielding. In Tyr, there could also be effects due to H-bonding; however, these are expected to be smaller than those in His/Trp since there is no tautomerism (as in His). The atom undergoing the H-bond interaction ( $\text{O}^\eta$ ) is far removed from  $\text{C}^\gamma$ , and  $\text{O}^\eta$  is almost always protonated, consistent with the shift range (Table S2, Supporting Information) for  $\text{C}^\zeta$  being small, both in proteins and these dipeptides. It thus appears that we need to do a better job of describing the “polar” interactions caused by the presence of the  $\text{NH}_3^+$  and  $\text{CO}_2^-$  groups and counterions. That is, we need to better account for electrostatic interactions.



**Table 1.** Experimental Chemical Shifts for the Nonprotonated C $\gamma$  in Phenylalanine and Tyrosine Model Compounds<sup>a</sup>

compound <sup>b</sup>	dipeptide	chemical shift (ppm)	compound <sup>b</sup>	dipeptide	chemical shift (ppm)
<b>1</b>	<b>Phe-Pro</b>	134.1	<b>7</b>	<b>Tyr-Glu</b>	123.2
<b>2</b>	<b>Phe-Phe</b>	135.3	<b>8</b>	<b>Tyr-Leu</b>	123.7
<b>3</b>	<b>Phe-Ala</b>	135.6	<b>18</b>	<b>Tyr-His</b>	124.2
<b>12</b>	<b>Phe-Leu</b>	135.7	<b>19</b>	<b>Tyr-Ile</b>	124.3
<b>13</b>	<b>Phe-Gly</b>	136.8	<b>9</b>	<b>Tyr-Phe</b>	124.7
<b>11</b>	<b>Phe-Tyr</b>	136.4	<b>20</b>	<b>Tyr-Trp</b>	125.2
<b>4</b>	<b>Phe-Val</b>	136.9	<b>21</b>	<b>Tyr-Gln</b>	125.7
<b>9</b>	<b>Tyr-Phe</b>	138.9	<b>22</b>	<b>Tyr-Gly</b>	126.5
<b>14</b>	<b>Ala-Phe</b>	139.2	<b>23</b>	<b>Gly-Tyr</b>	129.4
<b>5</b>	<b>Ile-Phe</b>	139.2	<b>24</b>	<b>Ala-Tyr</b>	129.5
<b>15</b>	<b>Arg-Phe</b>	139.6	<b>10</b>	<b>Leu-Tyr</b>	130.4
<b>2</b>	<b>Phe-Phe</b>	139.8	<b>11</b>	<b>Phe-Tyr</b>	130.8
<b>6</b>	<b>Gly-Phe</b>	140.3	<b>25</b>	<b>His-Tyr</b>	131.5
<b>16</b>	<b>Leu-Phe</b>	141.0	<b>26</b>	<b>Ile-Tyr</b>	132.4
<b>17</b>	<b>Tyr-Val</b>	123.0			

<sup>a</sup> Bold amino acid indicates amino acid of interest. <sup>b</sup> Structures are given in the Supporting Information, Figure S1.

**Table 2.** Experimental Chemical Shifts (in ppm) and Computed Chemical Shieldings (in ppm) for Phe-C $\gamma$  and Tyr-C $\gamma$  <sup>a</sup>

compound <sup>b</sup>	dipeptide	$\delta_{\text{expt}}$	HF-SCRF		B3LYP-SCRF	
			$\sigma_{\text{calcd}}$	$\delta_{\text{pred}}$	$\sigma_{\text{calcd}}$	$\delta_{\text{pred}}$
<b>1</b>	<b>Phe-Pro</b>	134.1	52.7	134.3	41.2	134.8
<b>2</b>	<b>Phe-Phe</b>	135.3	52.7	134.3	41.8	134.5
<b>3</b>	<b>Phe-Ala</b>	135.6	49.6	136.0	38.7	136.3
<b>11</b>	<b>Phe-Tyr</b>	136.4	52.3	134.5	40.6	135.2
<b>4</b>	<b>Phe-Val</b>	136.9	46.4	137.7	35.2	138.4
<b>9</b>	<b>Tyr-Phe</b>	138.9	44.6	138.7	33.0	139.8
<b>5</b>	<b>Ile-Phe</b>	139.2	40.7	140.8	30.6	141.2
<b>2</b>	<b>Phe-Phe</b>	139.8	41.9	140.1	32.3	140.1
<b>6</b>	<b>Gly-Phe</b>	140.3	45.2	138.4	34.4	138.9
<b>7</b>	<b>Tyr-Glu</b>	123.2	60.8	125.9	47.7	126.8
<b>8</b>	<b>Tyr-Leu</b>	123.7	64.1	123.4	51.3	123.9
<b>9</b>	<b>Tyr-Phe</b>	124.7	66.0	121.9	54.2	121.5
<b>10</b>	<b>Leu-Tyr</b>	130.4	56.1	129.6	43.5	130.2
<b>11</b>	<b>Phe-Tyr</b>	130.8	53.1	132.0	40.8	132.3

<sup>a</sup> Bold residue denotes the residue of interest. <sup>b</sup> Structures are given in the Supporting Information, Figure S1.

One possible way to include such effects into shielding calculations might be to use a self-consistent reaction field (SCRF) approach in which these effects are accounted for by means of a “solvent” model (e.g., a polarized continuum model, PCM), an approach that might reasonably be expected to reduce the computed shielding range to something more in line with experiment. We thus evaluated the effects of different dielectric constants of shielding (Supporting Information, Table S8), achieving convergence around  $\epsilon = 10$  (Supporting Information, Figure S2). We then used this value for the dielectric constant in further SCRF calculations. The results of calculations using the SCRF model and the Hartree–Fock method yielded a noticeable improvement, with  $R = 0.88$  and a slope =  $-1.85$ , over the use of supermolecule cluster calculations *in vacuo*, and the results from SCRF models using DFT were very similar ( $R = 0.88$ , slope =  $-1.66$ ). The best correlations between theory and experiment with the tyrosine dipeptides were obtained with the hydrogen-bond supermolecule cluster models with SCRF and are compared with results from the vacuum calculations in the Supporting Information, Table S9. A complete summary of the statistical results for the various sets of calculations is presented in Table S10, and the entire set of results from the HF-SCRF calculations and the B3LYP-SCRF calculations on both phenylalanine and tyrosine residues is presented in Table

2. The predicted chemical shifts for the (nonprotonated) C $\gamma$  atoms of tyrosine and phenylalanine can be obtained from the regression lines using the calculated shieldings, as follows:

$$\text{Phe C}\gamma \text{ (HF-SCRF): } \delta_{\text{pred}} = (301.2 - \sigma_{\text{calcd}})/1.85 \quad (1)$$

$$\text{Tyr C}\gamma \text{ (HF-SCRF): } \delta_{\text{pred}} = (222.0 - \sigma_{\text{calcd}})/1.28 \quad (2)$$

$$\text{Phe C}\gamma \text{ (DFT-SCRF): } \delta_{\text{pred}} = (265.0 - \sigma_{\text{calcd}})/1.66 \quad (3)$$

$$\text{Tyr C}\gamma \text{ (DFT-SCRF): } \delta_{\text{pred}} = (204.9 - \sigma_{\text{calcd}})/1.24 \quad (4)$$

The slopes, and consequently the intercepts or absolute shieldings, have obvious deficiencies;<sup>39</sup> however, as shown in Figure 3b, the predicted C $\gamma$  shifts are very well correlated with experiment (HF:  $R^2 = 0.94$ , rmsd = 1.6,  $N = 14$ ; DFT:  $R^2 = 0.92$ , rmsd = 1.7, covering a 17.1 ppm shift range). Similar predictions are obtained with the protein shift results (Supporting Information Table S11), and the combined peptide and protein shift results are compared in Figure 3c (HF,  $R^2 = 0.92$ , rmsd = 1.5,  $N = 32$ , over a 17.1 ppm chemical shift range). So, shifts can be calculated with, on average, an  $\sim 1.3$  ppm absolute error or accuracy, for phenylalanine and tyrosine C $\gamma$  in peptides and proteins, by using the methods described above.

Since the SCRF calculations improved the shift predictions for both phenylalanine and tyrosine, we also carried out SCRF calculations on the eight histidine dipeptides investigated previously,<sup>38</sup> to see if there were any improvements when using the SCRF approach. There were indeed small improvements (Supporting Information, Table S12) for each nonprotonated aromatic carbon. Specifically the  $R$  values become 0.97, 0.97, 0.83 for His C $\gamma$ , C $\delta^2$ , C $\epsilon^1$ , respectively, to be compared with the 0.94, 0.88, 0.82 values reported previously.<sup>4</sup> In addition, the SCRF calculations also provided a noticeable improvement in the slope for His C $\epsilon^1$ : from  $-1.54$  to  $-1.07$ . These results suggest that the type of SCRF calculation described here may be the most appropriate one for NMR shift predictions of aromatic amino acids in proteins as well as, potentially, for aromatic-containing enzyme inhibitors, such as some drug molecules.

We next consider the likely origins of the shift ranges seen with C $\gamma$  in Phe and Tyr and consider first the shielding tensor. We show in the Supporting Information Table S13 and Figure S3 the computed shielding tensor element magnitudes ( $\sigma_{11}$ ,  $\sigma_{22}$ , and  $\sigma_{33}$ ) as a function of the isotropic shielding ( $\sigma_{\text{iso}}$ ) for C $\gamma$  atoms of Phe and Tyr in dipeptides and in proteins. There are good correlations between  $\sigma_{ii}$  and  $\sigma_{\text{iso}}$  observed for  $\sigma_{22}$  ( $R = 0.96$ ) and  $\sigma_{11}$  ( $R = 0.87$ ), with the changes in  $\sigma_{\text{iso}}$  dominated by changes in  $\sigma_{22}$ . We then investigated the effects of inclusion of various structural features in different computational models (charged models, crystal structures without hydrogen-bond partners, hydrogen-bond models without SCRF, and HF-SCRF models) on the tensor magnitudes, as shown in Figure S4. As can be seen in Figure S4, there is essentially no change in  $\sigma_{33}$  between the different models, but  $\sigma_{22}$  varies considerably. Typical tensor orientations are shown in Figure 3d and e, for compounds **6** and **7**, which represent the least- and most-shielded C $\gamma$ , respectively. As expected, the  $\sigma_{33}$  element in our dipeptide systems is oriented perpendicular to the aromatic ring, while

(39) Jameson, A. K.; Jameson, C. J. *Chem. Phys. Lett.* **1987**, 134, 461.

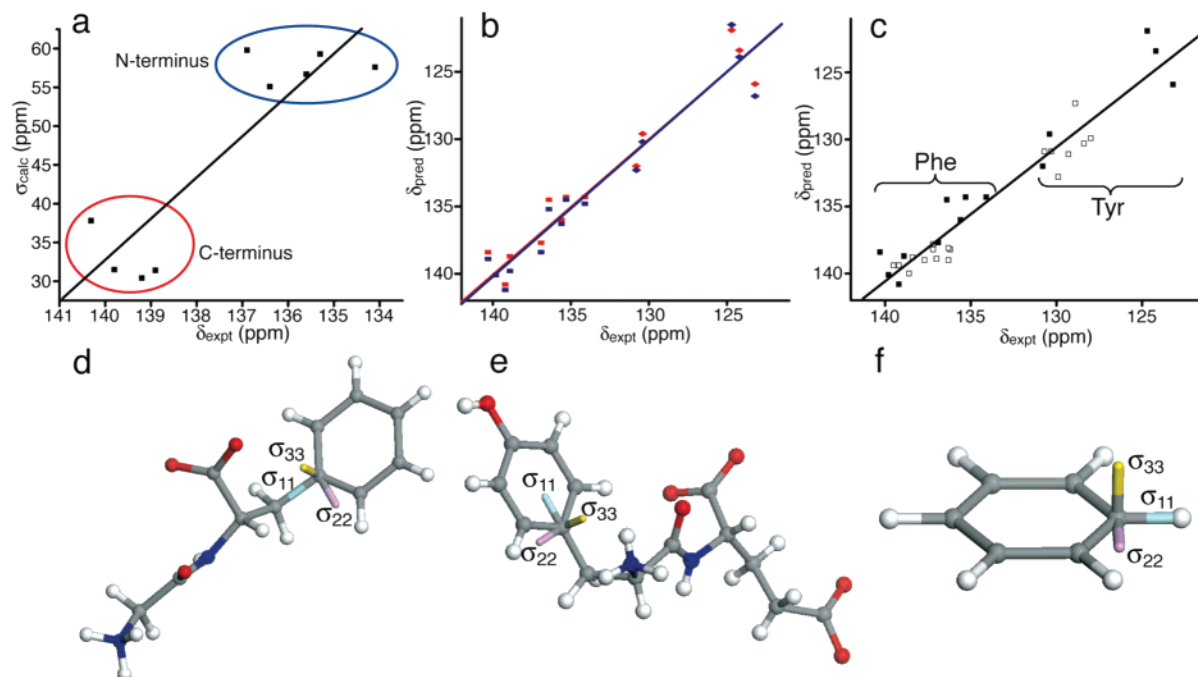


**Figure 3.**  $^{13}\text{C}$  chemical shifts and shielding tensor orientations: (a) Correlation between the calculated shielding and experimental shifts for the charged models; (b) Plot of predicted versus experimental chemical shifts for  $\text{C}'$  in Phe and Tyr dipeptides (red, HF-SCRF; blue, B3LYP-SCRF; squares, phenylalanine shifts; diamonds, tyrosine shifts); (c) Plot of predicted versus experimental chemical shifts for  $\text{C}'$  of Phe and Tyr in dipeptides and proteins (filled squares, dipeptide data; open squares, protein data); (d) Orientations of the shielding tensor elements of  $\text{C}'$  atom in Gly-Phe (**6**); (e) in Tyr-Glu (**11**); and (f) in benzene.

$\sigma_{11}$  is along the  $\text{C}'\text{--C}^\beta$  bond vector (as is the case in benzene, Figure 3f). Interestingly, even though the magnitudes of  $\sigma_{11}$  and  $\sigma_{22}$  change considerably from one dipeptide to another ( $\Delta\sigma_{11}$ :  $\sim 12$  ppm in Phe and Tyr;  $\Delta\sigma_{22}$ : 29 ppm in Phe and 38.5 ppm in Tyr), there is essentially no change in their orientation between the different structures, the same result as that observed in tryptophan dipeptides.<sup>2</sup> However, this observation is different from the situation found in the histidine dipeptides,<sup>38</sup> where there is a rotation of  $\sigma_{11}$  and  $\sigma_{22}$  in the plane of the aromatic ring, due most likely to the presence of a nitrogen ( $\text{N}^{\delta 1}$ ) involved in hydrogen-bond formation with neighboring molecules, in the imidazole ring.

So, in Phe and Tyr, changes in the isotropic chemical shift are due to changes in  $\sigma_{22}$  and  $\sigma_{11}$ , with  $\sigma_{33}$  being essentially constant. This observation, together with the observation that the computed shifts are highly sensitive to the presence of nearby charges, which influence  $\sigma_{22}$  and  $\sigma_{11}$ , suggested to us the following possibility: that the changes in isotropic shift seen experimentally are due to electrostatic field effects which change the  $\pi$ -electron density in the aromatic ring, influencing the atomic charge on  $\text{C}'$  and its shielding. We thus next evaluated the  $\text{C}'$  atomic charges using a natural bonding orbital (NBO) analysis,<sup>40</sup> in both peptides and proteins. As can be seen in Figure 4a (and Table S14 in the Supporting Information), there is a very good correlation ( $R = 0.93$ ) between the NBO atomic charge and chemical shift for Phe  $\text{C}'$  and Tyr  $\text{C}'$  in both peptides and proteins. In all cases, the residues having the larger negative atomic charges are more shielded than those having the less negative charge. In very early work it was found in a variety of  $4n + 2$  ( $n = 0, 1, 2$ )  $\pi$ -electron aromatic systems<sup>10–14</sup> that the isotropic  $^{13}\text{C}$  NMR chemical shifts were highly correlated with  $\pi$  electron densities (from Hückel calculations). An increase in  $\pi$  electron density would be expected, qualitatively, to increase

the atomic charge on  $^{13}\text{C}$  and result in increased shielding, and this was indeed seen, there being a slope of  $\sim 160$  ppm/e.<sup>10–14</sup> This then raises the following question: are the changes in Phe and Tyr  $\text{C}'$  shifts we see (due to the presence of near-neighbor charged or polar residues) basically the same as those seen in, e.g., the cyclooctadiene dianion ( $4n + 2 = 10$ , a formal charge on carbon  $\approx 2e/8 = 0.25$  e) or the cyclopropyl cation ( $4n + 2 = 2$ , formal charge on carbon  $\approx 1/3$ )? We therefore computed the shielding tensors and NBO charges for the tropylium cation, benzene, and the cyclopentadienide anion and compared the results obtained with those determined from experiment,<sup>41</sup> finding a very good correlation ( $R^2 = 0.99$ , slope =  $-1.1$ ) (Figure 4b). The NBO charges for these and several other aromatic species (Supporting Information Table S15) were also found to be highly correlated with the computed isotropic shieldings (Supporting Information Figure S5) but were uniformly offset (by  $\sim 35$  ppm) from the computed Phe, Tyr results. We thus next computed the shieldings/NBO charges for a second series of compounds, Supporting Information Table S16, which contained methyl substitutions at  $\text{C}1$ , in order to better simulate the effect of the alkyl substituent present at  $\text{C}'$  of Phe and Tyr. As shown in Figure 4c, when the Phe, Tyr  $\text{C}'$ , and other aromatic shieldings are plotted as a function of the computed NBO charges, the two data sets are essentially indistinguishable and strongly support the idea that increasing  $^{13}\text{C}$  atomic charge due to electrostatic interactions (in peptides and proteins) results in increased shielding. That is, these results strongly support the idea that changes in  $\pi$  electron density in peptides and proteins, due to electrostatic field effects, result in changes in the

(40) Glendening, E. D.; Reed, A. E.; Carpenter, J. E.; Weinhold, F. *NBO*, version 3.1; Theoretical Chemistry Institute: University of Wisconsin, Madison, WI.

(41) Strub, H.; Beeler, A. J.; Grant, D. M.; Michl, J.; Cutts, P. W.; Zilm, K. W. *J. Am. Chem. Soc.* **1983**, *105*, 3333.

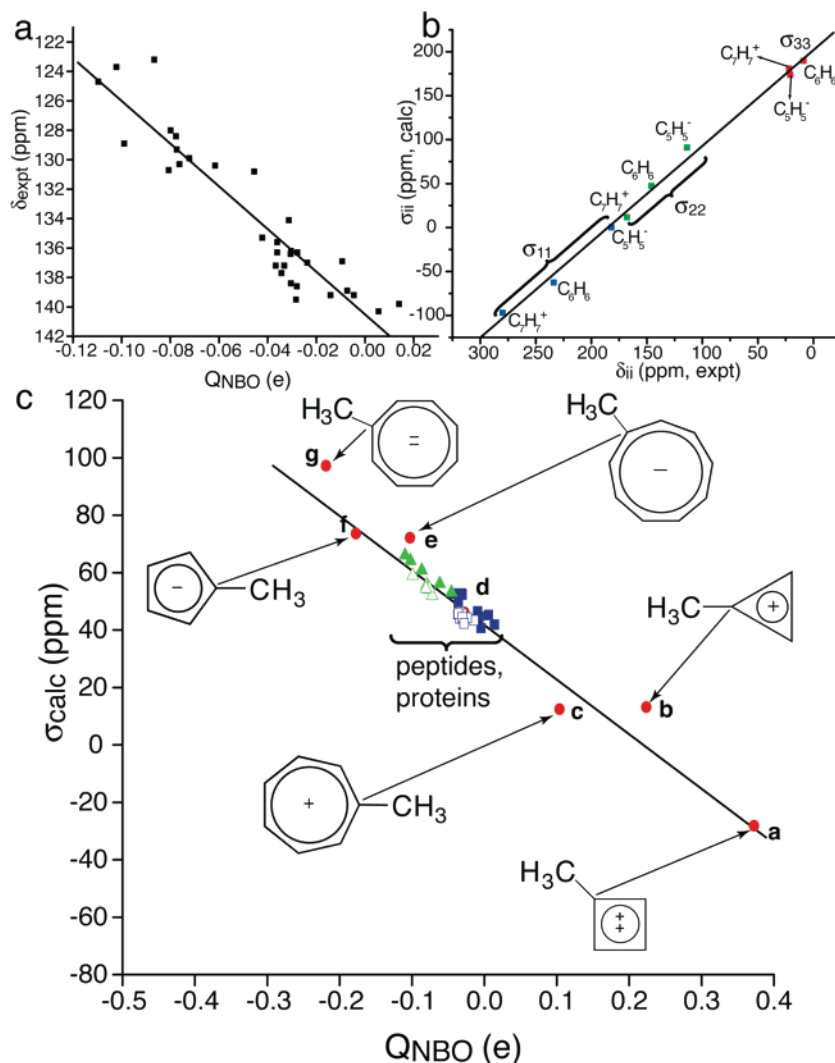
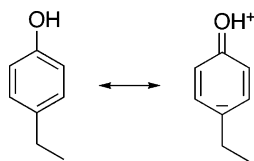


**Figure 4.** Correlations between shifts (shielding) and NBO charge: (a) Plot of experimental  $^{13}\text{C}$  NMR shifts versus carbon NBO charges for  $\text{C}\gamma$  of Phe and Tyr in peptides and proteins; (b) Plot of the computed shielding tensor element magnitudes of aromatic systems ( $\text{C}_7\text{H}_7^+$ ,  $\text{C}_6\text{H}_6$ ,  $\text{C}_5\text{H}_5^-$ ) versus the respective experimental values; (c) Plot of the calculated  $\text{C}\gamma$  chemical shieldings versus  $\text{C}\gamma$  NBO charges for Phe and Tyr residues in peptides and proteins and in various aromatic ring systems: a, methylcyclobutadiene dication; b, methylcyclopropenium; c, methyltropylium; d, toluene; e, methylcyclononatetraenyl; f, methylcyclopentadienide; g, methylcyclooctatetraenyl dianion) (green filled triangles, tyrosine dipeptides; green open triangles, tyrosine residues in proteins; blue filled squares, phenylalanine dipeptides; blue open squares, phenylalanine residues in proteins). The slope of the correlation through all the data points is 191 ppm/e.

formal atomic charges on  $^{13}\text{C}\gamma$  which are highly correlated with shielding. A larger charge density on  $\text{C}\gamma$  is seen in N-terminal peptides and correlates with increased shielding (Figures 4a, 2e, 2f), while the opposite effect is seen with the C-terminal residues. In the case of the peptides (and proteins), these charge effects are of course in general much smaller than those seen with the formally charged species (Figure 4c), although the shift/charge density of the methyl nonatetraene monoanion ( $4n + 2 = 1$ ,  $1e/9 \approx 0.11e$ ) does in fact overlap that found in the most highly shielded Tyr residues, where resonance likely plays an important role, enhancing the charge on  $\text{C}\gamma$ .



So, while there are no formal charges on the aromatic rings in Phe and Tyr, the uniform shielding in Tyr over Phe may be

attributable, at least in part, to this enhanced atomic charge. We thus propose that there are two contributors to the  $^{13}\text{C}$  shifts in Phe and Tyr in peptides and proteins: an electrostatic field effect from charged or polar groups and, for Tyr, a resonance effect. Increasing the  $\pi$  electron density results in increases in the NBO charge on  $\text{C}\gamma$  and an increase in isotropic shielding (due to changes in  $\sigma_{22}$  and  $\sigma_{11}$ , Supporting Information Figure S6), with the correlation between isotropic shielding and NBO charge being essentially the same as that seen in other aromatic systems, containing three to nine carbon atoms, Figure 4c. These effects are not observed (or are much less apparent) in the other aromatic amino acids, where the presence of heteroatoms in the aromatic rings leads to tautomerism and/or strong local hydrogen-bond interactions.

### Conclusion

The results we have described above are of interest for a number of reasons. First, we have obtained the  $^{13}\text{C}$  solid-state MAS NMR shifts of the nonprotonated  $\text{C}\gamma$  atom from 26 phenylalanine and tyrosine containing dipeptides. The  $\text{C}\gamma$

chemical shifts display a smaller range (6.9–9.4 ppm) than those observed in ring nitrogen containing aromatic amino acids (Trp and His, ~11.0–14.0 ppm). The values of the C $\gamma$  shifts in the dipeptides are larger than the ranges seen in proteins (3.7–7.2 ppm). Second, we have used quantum chemical methods to investigate these C $\gamma$  shifts, in both dipeptides and proteins. The results obtained highlight the importance of including hydrogen-bond partners and the use of a self-consistent reaction field method to better describe the electrostatic interactions, in both peptides and proteins. Third, we found that the C $\gamma$  shieldings were highly correlated with C $\gamma$  atomic charges. This suggests a general model for C $\gamma$  shifts in Phe and Tyr in which electrostatic interactions with neighboring groups or residues affect  $\pi$  electron densities and C $\gamma$  atomic charges, with enhanced charges correlating with increased shielding, as seen in previous studies of other  $4n + 2$  aromatic  $\pi$  electron systems<sup>10–14</sup> containing three to nine carbons. Taken together these results are of general interest in the context of NMR and quantum chemical studies

of <sup>13</sup>C NMR chemical shifts, bringing together, in an interesting and unexpected way, results from systems as diverse as lysozyme and the tropylium cation.

**Acknowledgment.** We thank Scott Wilson for his help with the crystallography and powder diffraction. This work was supported by the United States Public Health Service (NIH Grant GM50694). The Materials Chemistry Laboratory at the University of Illinois was supported in part by Grants NSF CHE 95-03145 and NSF CHE 03-43032 from the National Science Foundation.

**Supporting Information Available:** Additional results (Tables S1–S16 and Figures S1–S6) and the CIF files of the two new crystal structures reported in this paper. This material is available free of charge via Internet at <http://pubs.acs.org>.

JA071227Y